
iMixer: hierarchical Hopfield network implies an invertible, implicit and iterative MLP-Mixer

Toshihiro Ota
CyberAgent

ota_toshihiro@cyberagent.co.jp

Masato Taki
Rikkyo University

taki_m@rikkyo.ac.jp

Abstract

In the last few years, the success of Transformers in computer vision has stimulated the discovery of many alternative models that compete with Transformers, such as the MLP-Mixer. Despite their weak inductive bias, these models have achieved performance comparable to well-studied convolutional neural networks. Recent studies on modern Hopfield networks suggest the correspondence between certain energy-based associative memory models and Transformers or MLP-Mixer, and shed some light on the theoretical background of the Transformer-type architectures design. In this paper, we generalize the correspondence to the recently introduced hierarchical Hopfield network, and find *iMixer*, a novel generalization of MLP-Mixer model. Unlike ordinary feedforward neural networks, iMixer involves MLP layers that propagate forward from the output side to the input side. We characterize the module as an example of invertible, implicit, and iterative mixing module. We evaluate the model performance with various datasets on image classification tasks, and find that iMixer, despite its unique architecture, exhibits stable learning capabilities and achieves performance comparable to or better than the baseline vanilla MLP-Mixer. The results imply that the correspondence between the Hopfield networks and the Mixer models serves as a principle for understanding a broader class of Transformer-like architecture designs.

1 Introduction

The Transformer architecture [1], which has achieved great success in natural language processing in recent years, has proven to perform well in a wide range of computer vision tasks such as image recognition and object detection. One example is the Vision Transformer (ViT) [2, 3], a standard Transformer architecture applied to image classification that achieves performance competitive with state-of-the-art convolutional neural networks (CNNs). More recently, alternative models of ViT have been discovered that do not use attention mechanism such as the MLP-Mixer [4, 5]. MLP-Mixer learns long-range dependencies between tokens (patches) using only a simple MLP instead of attention mechanism. Such alternative models are now collectively referred to as MetaFormers [6, 7], see Fig. 1a. Although a number of ViT variants have been proposed and the performance of them continues to improve, developments in their architectural design are somewhat heuristic and a prospective perspective for design is desired.

The Hopfield network is a classical associative memory model of neural networks [8, 9]. Recent studies on modern Hopfield networks suggest the correspondence between certain energy-based associative memory models and Transformers or MLP-Mixer [10–12], which is a promising candidate for a unified description of Transformer’s architectural design. In this paper, we extend the correspondence to the recently introduced hierarchical Hopfield network [13] and show that this extension results in a new class of MLP-Mixer architectures, the *iMixer*. The macro-architecture design of iMixer is the same as that of MLP-Mixer and Transformers (MetaFormers), consisting of stacked token- and channel-mixing blocks. However, iMixer differs significantly from MLP-Mixer

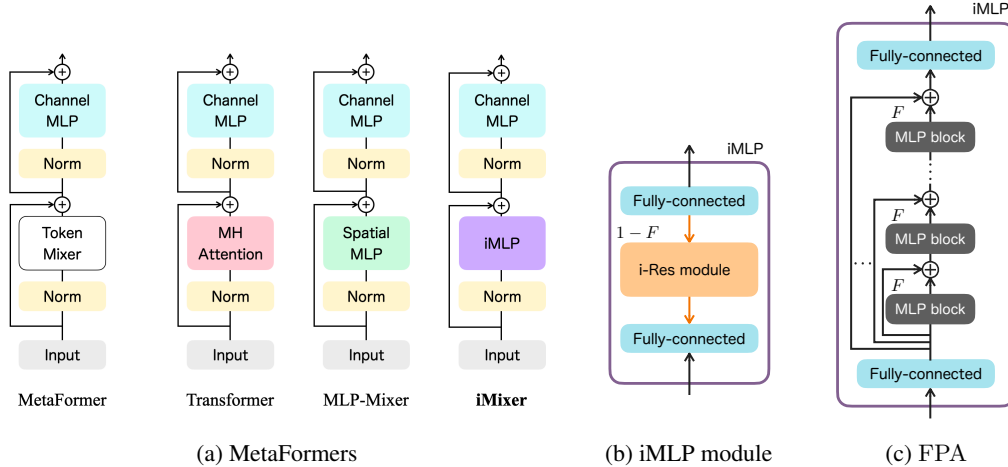


Figure 1: (a) Macro-architecture design of the Transformer-type networks and (b) the structure of iMLP module. (c) Restricting to invertible $(1 - F)$ yields the feedforward realization of the iMLP module using the fixed-point approximation (FPA).

and ViT in that the token-mixing block is composed of the invertible ResNet (i-Res) module, or infinitely deep neural network [14–16], see Fig. 1b. Although this architectural design is completely unexpected from the computer vision perspective, it is a natural consequence of multi-layering from the Hopfield network side. By exploiting the correspondence, we systematically obtain models that have been missed in previous architectural designs.

We show that the dynamics of the hierarchical Hopfield network implies iMixer whose token-mixing module is defined as an MLP $f(\cdot)$ that propagates forward from the output side y to the input side x as $x = f(y)$. The module that cannot be explicitly written down in a forward propagation equation from the input side to the output side is an example of the implicit neural network [16]. Our iMixer is a new type of MetaFormer that uses a mixing module composed of implicit neural networks. In our case, the implicit structure can be written by inserting $x = f(y)$, a forward propagation in the opposite direction. Using the i-Res module, this backward-forward propagation can be represented as a normal forward propagating neural network with infinitely iterated layers as shown in Fig. 1c. In turn, this representation enables us to easily implement and train the model as a usual feedforward neural network.

Our proposed architecture is not only novel in design, but is actually based on theoretical derivations from the hierarchical Hopfield network. By conducting multiple rounds of training on image recognition tasks and obtaining statistics on validation performance, we also verify that changing the token-mixing modules in MLP-Mixer to the inverted mixing module (iMLP module) can improve the performance of the model. This result suggests a new direction for image recognition architecture design using implicit modules. The main contributions of the paper is summarized as follows:

- The primary contribution is the proposal of a new direction for MetaFormer model design, facilitated by the novel Hopfield/Mixer correspondence. Our intention is to provide a first step towards a theoretical underpinning for MetaFormers.
- Our second contribution is the theoretical derivation of a specific new MetaFormer model (iMixer), based on the Hopfield/Mixer correspondence. This work is the first example to *predict* a novel MetaFormer model from modern Hopfield networks. In the theoretical formulation, the proposed model naturally incorporates an implicit module $(1 - F)^{-1}$, which may initially appear unconventional from a computer vision perspective.
- While a theoretical derivation of a deep learning model may be apt to a mere and impractical proposition, our empirical study supports the validity of the proposed iMixer as a novel and meaningful MetaFormer, which can be considered our third contribution.

2 Related Work

Transformer & Mixer models. Transformer [1], which has proven its effectiveness in natural language processing, is now widely used in computer vision. ViT [2] is an alternative model to CNN that uses Transformer encoders for image recognition and demonstrates the effectiveness of Transformer in computer vision. Various improved versions of ViT have also been proposed, such as incorporating local structure in attention or using distillation [3].

While it is widely believed that an attention mechanism is critical to the success of ViT, there are results that cast doubt on its necessity; MLP-Mixer [4, 17, 5, 18] has shown that by simply replacing the attention mechanism of ViT with MLP, it is possible to achieve performance approaching that of ViT. This discovery has stimulated a series of studies that have shown that a wide range of token-mixing mechanisms, including pooling [6], global filtering [19], recurrent layers [20], and graph neural networks [21], can be used as substitutes for the attention mechanism. These findings suggest that, in fact, in computer vision, it is not the attention mechanism itself that is important, but the macro-architecture design of the Transformer, which repeatedly mixes tokens and channels. These groups of models are referred to as MetaFormers [6, 7].

Classical & modern Hopfield networks. The Hopfield network is a well-known model for associative memory in neural networks [8, 9]. In this network, stored memories and their retrieval are described by the attractors of an energy function and the dynamics converging to them. In practice, however, the classical Hopfield network is known to suffer from a limited memory capacity. To address this issue, models with substantially higher memory capacities have recently been proposed [22–24], but they are supposed to have many-body interactions among neurons, which is biologically implausible in the brain.

Close to the time when these modern Hopfield networks were proposed, Ramsauer et al. found that each of the attention modules in the Transformer can essentially be identified with the process of the update rule of a certain continuous Hopfield network [11], and their algorithm has been developed and applied to some tasks with success [25–27]. Based on these heuristic findings and earlier works, Krotov and Hopfield developed more comprehensive associative memory models, which consist of visible and hidden neurons with only two-body interactions between them [10, 13]. In their papers, Krotov and Hopfield demonstrated that many of modern neural network models in the literature can be derived from Hopfield-type networks equipped with Lagrangians that define the systems.

Implicit deep learning. Implicit neural networks and implicit layers have been discussed in various papers [16, 15, 28–32]. Implicit layer generally refers to a layer that cannot be written as an explicit forward propagation expression, such as $y = f(x)$, but is expressed as an implicit expression $g(x, y) = 0$.

The invertible ResNet layer [14] used in this paper is also a layer related to implicit layers. In this paper, we consider a layer in which the propagation from the output side y to the input side x is represented by the invertible ResNet layer $x = y + F(y)$. A fixed-point iteration method can be used to represent this layer in the usual orientation. The resulting forward propagation equation is $y = x - F(x - F(\dots))$, an infinitely deep network that iteratively adapts the same layer as depicted in Fig. 1c. In other words, this forward propagation cannot be expressed in terms of ordinary finite layers.

The deep equilibrium model (DEQ) [15, 30] proposed a new computer vision architecture by introducing an implicit layer defined by fixed point for iterative application of a layer. The iterative layer structure of iMixer has similarities with this study. Unlike DEQ, which uses back propagation with implicit differentiation using the Jacobian, iMixer simply trains the entire model end-to-end using the usual gradient descent method.

3 Background

To fix notations, we here provide a derivation of the MLP-Mixer [4] from a continuous Hopfield network.

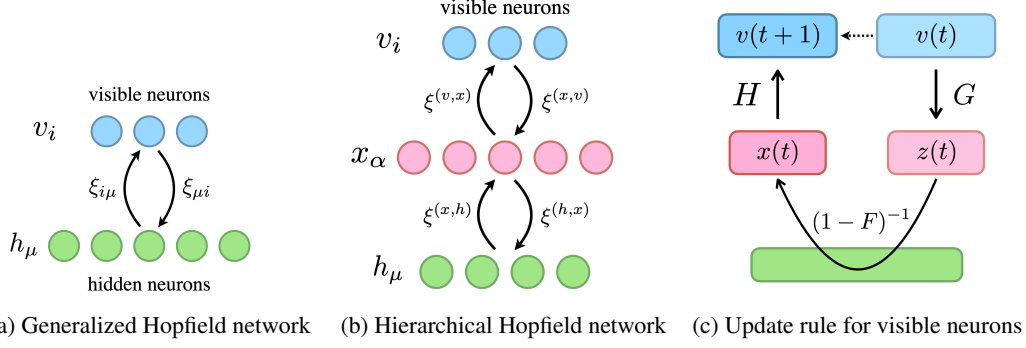


Figure 2: Modern Hopfield networks.

3.1 Overview of the generalized Hopfield network

Let us first briefly review the generalized Hopfield network proposed in [10]. In this system, the dynamical variables are composed of N_v visible neurons and N_h hidden neurons both continuous,

$$v(t) \in \mathbb{R}^{N_v}, \quad h(t) \in \mathbb{R}^{N_h}, \quad (1)$$

where the argument t can be thought of as “time”. The interaction matrices between them,

$$\xi \in \mathbb{R}^{N_h \times N_v}, \quad \tilde{\xi} \in \mathbb{R}^{N_v \times N_h}, \quad (2)$$

are basically supposed to be symmetric: $\tilde{\xi} = \xi^\top$, see Fig. 2a. With the relaxing time constants of the two groups of neurons τ_v and τ_h , the system is described by the following differential equations,

$$\tau_v \frac{dv_i(t)}{dt} = \sum_{\mu=1}^{N_h} \xi_{i\mu} f_\mu(h(t)) - v_i(t), \quad (3)$$

$$\tau_h \frac{dh_\mu(t)}{dt} = \sum_{i=1}^{N_v} \xi_{\mu i} g_i(v(t)) - h_\mu(t), \quad (4)$$

where the activation functions f and g are determined through Lagrangians $L_h : \mathbb{R}^{N_h} \rightarrow \mathbb{R}$ and $L_v : \mathbb{R}^{N_v} \rightarrow \mathbb{R}$, such that

$$f_\mu(h) = \frac{\partial L_h(h)}{\partial h_\mu}, \quad g_i(v) = \frac{\partial L_v(v)}{\partial v_i}. \quad (5)$$

The canonical energy function for this system is given by

$$E(v, h) = \sum_{i=1}^{N_v} v_i g_i(v) - L_v(v) + \sum_{\mu=1}^{N_h} h_\mu f_\mu(h) - L_h(h) - \sum_{\mu,i} f_\mu \xi_{\mu i} g_i. \quad (6)$$

One can easily find that this energy function monotonically decreases along the trajectory of the dynamical equations to define an associative memory model,

$$\frac{dE(v(t), h(t))}{dt} \leq 0, \quad (7)$$

provided that the Hessians of the Lagrangians are positive semi-definite. In addition to this, if the overall energy function is bounded from below, the trajectory is guaranteed to converge to a fixed point attractor state, which corresponds to one of the local minima of the energy function. Such fixed points and the process of convergence are thought of as associative memories and memory retrieval of an associative memory model. The formulation of neural networks in terms of Lagrangians and the associated energy functions enables us to easily experiment with different choices of the activation functions and different architectural arrangements of neurons.

3.2 MLP-Mixer as an associative memory model

Suppose we have a fixed interaction matrix $\xi_{\mu i}$, then the system is defined by the choice of Lagrangians L_h and L_v . Tang and Kopp demonstrated that the specific choice of Lagrangians called “model C” in [10] essentially reproduces the mixing layers in the MLP-Mixer [12], which is given by the following Lagrangians:

$$L_h(h) = \sum_{\mu} \phi(h_{\mu}), \quad L_v(v) = \sqrt{\sum_i (v_i - \bar{v})^2}, \quad (8)$$

where ϕ will be specified below, and $\bar{v} = \sum_i v_i / N_v$. For these Lagrangians, the activation functions are

$$f_{\mu}(h) = \frac{\partial L_h}{\partial h_{\mu}} = \phi'(h_{\mu}), \quad (9)$$

$$g_i(v) = \frac{\partial L_v}{\partial v_i} = \frac{v_i - \bar{v}}{\sqrt{\sum_j (v_j - \bar{v})^2}} = \text{LayerNorm}(v)_i. \quad (10)$$

We now consider the adiabatic limit, $\tau_v \gg \tau_h$, which means that the dynamics of the hidden neurons is much faster than that of the visible neurons, i.e., we can take $\tau_h \rightarrow 0$:

$$\text{Eq. (4)} \quad \rightsquigarrow \quad h_{\mu}(t) = \sum_{i=1}^{N_v} \xi_{\mu i} \text{LayerNorm}(v(t))_i. \quad (11)$$

Substituting the above expression into the other dynamical equation, we find

$$\tau_v \frac{dv_i(t)}{dt} = \sum_{\mu} \xi_{i\mu} \phi' \left(\sum_j \xi_{\mu j} \text{LayerNorm}(v(t))_j \right) - \alpha v_i(t). \quad (12)$$

Notice that we can put an arbitrary coefficient α , which can be even zero, in front of the decay term, since for this choice of Lagrangian L_v its Hessian has a zero mode:

$$\sum_j M_{ij}(v_j - \bar{v}) = 0, \quad M_{ij} := \frac{\partial^2 L_v}{\partial v_i \partial v_j}. \quad (13)$$

If we take $\alpha = 0$ and discretize the differential equation by taking $\Delta t = \tau_v$, then we obtain the update rule for the visible neurons,

$$v_i(t+1) = v_i(t) + \sum_{\mu} \xi_{i\mu} \sigma \left(\sum_j \xi_{\mu j} \text{LayerNorm}(v(t))_j \right), \quad (14)$$

where we defined $\sigma := \phi'$. If one chooses $\sigma = \text{GELU}$, this update rule is identified with the token- and channel-mixing blocks in the mixing layers discussed in [4]. We will utilize this fact in Sec. 4.1.

4 Model

Along the line of [10], Krotov further extended the model in such a way that the generalized Hopfield network can consist of multiple hidden layers [13], which we refer to as the hierarchical Hopfield network. Based on the result in Sec. 3.2 and Krotov’s extension, in this section we propose an invertible, implicit and iterative MLP-Mixer (iMixer), a generalization of the MLP-Mixer with multiple hidden layers.

As one of the simplest generalizations in view of the hierarchical Hopfield network, we consider the case of three layers in total,¹ which consists of one visible layer with N_v neurons and two hidden layers with N_x and N_h neurons for each, as shown in Fig. 2b. The dynamics of this system is then

¹For more general cases, see Appendix B.

described by the following differential equations [13],

$$\tau_v \frac{dv_i(t)}{dt} = \sum_{\alpha=1}^{N_x} \xi_{i\alpha}^{(v,x)} e_\alpha(x(t)) - v_i(t), \quad (15)$$

$$\tau_x \frac{dx_\alpha(t)}{dt} = \sum_{i=1}^{N_v} \xi_{\alpha i}^{(x,v)} g_i(v(t)) + \sum_{\mu=1}^{N_h} \xi_{\alpha\mu}^{(x,h)} f_\mu(h(t)) - x_\alpha(t), \quad (16)$$

$$\tau_h \frac{dh_\mu(t)}{dt} = \sum_{\alpha=1}^{N_x} \xi_{\mu\alpha}^{(h,x)} e_\alpha(x(t)) - h_\mu(t), \quad (17)$$

where $\xi^{(A,B)}$ indicates the interaction from B neurons to A neurons: $\xi^{(A,B)} \in \mathbb{R}^{N_A \times N_B}$, and the activation functions are again determined through each of the Lagrangian,

$$f_\mu(h) = \frac{\partial L_h(h)}{\partial h_\mu}, \quad g_i(v) = \frac{\partial L_v(v)}{\partial v_i}, \quad e_\alpha(x) = \frac{\partial L_x(x)}{\partial x_\alpha}. \quad (18)$$

4.1 iMixer: invertible, implicit and iterative MLP-Mixer

In order to derive iMixer, we take our Lagrangians as follows:

$$L_h(h) = \sum_{\mu} \phi_h(h_\mu), \quad L_v(v) = \sqrt{\sum_i (v_i - \bar{v})^2}, \quad L_x(x) = \sum_{\alpha} \phi_x(x_\alpha), \quad (19)$$

where $\bar{v} = \sum_i v_i / N_v$ and the activation function for the visible neurons reads $g_i = \text{LayerNorm}(\cdot)_i$. Hence by following the same discussion as in Sec. 3.2, the dynamical equation for the visible neurons eventually becomes a residual network,

$$v_i(t+1) = v_i(t) + \sum_{\alpha=1}^{N_x} \xi_{i\alpha}^{(v,x)} e_\alpha(x(t)). \quad (20)$$

To obtain the time evolution for $x(t)$ and to solve the whole update rule, we again consider the adiabatic limit, $\tau_v \gg \tau_x \gg \tau_h$, then the dynamical equations for the hidden neurons are reduced to

$$x_\alpha(t) = \sum_{i=1}^{N_v} \xi_{\alpha i}^{(x,v)} \text{LayerNorm}(v(t))_i + \sum_{\mu=1}^{N_h} \xi_{\alpha\mu}^{(x,h)} f_\mu(h(t)), \quad (21)$$

$$h_\mu(t) = \sum_{\alpha=1}^{N_x} \xi_{\mu\alpha}^{(h,x)} e_\alpha(x(t)). \quad (22)$$

By substituting Eq. (22) to the other, one obtains

$$x(t) - \xi^{(x,h)} f(\xi^{(h,x)} e(x(t))) = \xi^{(x,v)} \text{LayerNorm}(v(t)), \quad (23)$$

where we switched to the vector and matrix notation for simplicity. Note that all the products here are matrix multiplication. For this expression, we define a contractive MLP block $F : \mathbb{R}^{N_x} \rightarrow \mathbb{R}^{N_x}$ and a fully-connected layer $G : \mathbb{R}^{N_v} \rightarrow \mathbb{R}^{N_x}$ as

$$F := (\xi^{(x,h)} f) \circ (\xi^{(h,x)} e), \quad G := \xi^{(x,v)} \text{LayerNorm}(\cdot), \quad (24)$$

and write

$$(1 - F)(x(t)) = G(v(t)) =: z(t). \quad (25)$$

Combining Eqs. (25) and (20), we obtain the update rule for the visible neurons depicted as in Fig. 2c:

$$v(t+1) = v(t) + H(x(t)), \quad (26)$$

$$x(t) = (1 - F)^{-1}(z(t)), \quad (27)$$

$$z(t) = G(v(t)), \quad (28)$$

Algorithm 1 Feedforward computation of the iMLP module.

Input: input x , fully-connected layer G , contractive MLP block F , fully-connected layer H , number of fixed-point iterations n
Init: $x^0 := G(x)$
for $a = 0, \dots, n - 1$ **do**
 $x^{a+1} := x^0 + F(x^a)$
end for
return: $H(x^n)$

where $H := \xi^{(v,x)}e(\cdot)$. The activation functions $f = \phi'_h$ and $e = \phi'_x$ need not be specified at this stage. In practice, we will fix them to a neuron-wise activation $f = e = \text{GELU}$ in experiments to compare with the vanilla MLP-Mixer.

To fully solve the update rule for the visible neurons, we need to compute the inverse of the residual connection $(1 - F)^{-1}$ in Eq. (27), which is generically intractable. To resolve this difficulty, we employ the fixed-point iteration method for residual connections provided by [14]; we set $x^0 = z(t)$ and perform the fixed-point iterations for some integer n as follows:

$$x^{a+1} = x^0 + F(x^a), \quad F = (\xi^{(x,h)}f) \circ (\xi^{(h,x)}e), \quad (29)$$

for $a = 0, \dots, n - 1$. Behrmann et al. showed that this sequence of operations makes x^a converge to $x(t)$ exponentially fast with respect to n owing to the Banach fixed-point theorem. We thus can approximate $x(t) \simeq x^n$ and numerically solve the update rule, as shown in Algorithm 1. Figure 1b illustrates our inverted mixing module (iMLP module) using the i-Res module, and the whole iMixer architecture is composed of those as token-mixing modules,

$$v(t + 1) = v(t) + \xi^{(v,x)} \text{GELU} \left(\text{FPA} \left(\xi^{(x,v)} \text{LN}(v(t)) \right) \right), \quad (30)$$

where the activation functions f and e are taken to be GELU here, and FPA indicates the fixed-point approximation of the operation $(1 - F)^{-1}$. Thus the FPA layer Eq. (29) in the iMLP module that maps $z(t) = x^0$ to $x(t) \simeq x^n$ is implemented as a deep feedforward network that applies the same layer $F(\cdot)$ n times as in Fig. 1c.

Through the recursive operations in FPA, features and the gradients could explode with increasing iterations and hence it can cause instabilities during training. To avoid such a serious issue, we will follow the prescription employed in the original paper [14] referred to as the spectral normalization, which serves to stabilize the training process (and also inference) by normalizing the spectrum of the weight matrices.

Our update rule for the visible neurons, as well as the fixed-point iteration method performed in FPA, can be regarded as a form of the deep equilibrium model or the implicit layer [15, 16]. In such algorithms also, the solution converges to a fixed point, but they do not necessarily have a direct gradient descent method for training.

5 Experiments

In order to verify the validity of the iMLP module based on the correspondence with the Hopfield network side, in this section we embed the module into MLP-Mixer, which we refer to as iMixer, and perform several experiments to compare our iMixer with the vanilla MLP-Mixer (Mixer). In the main part of the experiments, we utilize the CIFAR-10 dataset [33] to evaluate the performance of iMixer-Small (S), -Base (B) and -Large (L) models corresponding to the vanilla Mixer models. We use PyTorch Image Models `timm` [34] to implement the models in all the experiments.² The experimental details are provided in Appendix C.

Network architecture. We incorporate the iMLP module Eq. (30) with the token-mixing blocks, and the rest of the iMixer has exactly the same structure as the vanilla Mixer. That brings in the following additional hyperparameters to iMixer: the dimension of the hidden neurons N_h , the number of fixed-point iteration n , and the number of power-iteration n_p and the coefficient $c (< 1)$ for the

²The code is available at <https://github.com/Toshihiro-Ota/imixer>.

Table 1: Top-1 accuracy (%) of iMixer ($h_r = 2, n = 2$), compared with the vanilla Mixer.

Model	Small	Base	Large
Mixer (baseline)	88.08 \pm 0.51	89.03 \pm 0.24	86.67 \pm 0.30
iMixer (ours)	88.56 \pm 0.30	89.07 \pm 0.33	87.48 \pm 0.40

spectral normalization. The large number of power-iteration n_p stabilizes the training of the models with the i-Res module. Based on the successful practices reported in [14], we will fix $n_p = 8$ and $c = 0.9$ in the experiments. The effect of the spectral normalization will be discussed later in Sec. 5.2. As we take the dimension of the middle neurons equal to the usual spatial MLP dimension: $N_x = D_S$, the dimension of the hidden neurons as a hyperparameter is specified by the ratio to D_S , that is, we have a hyperparameter h_r defined by $h_r := N_h/D_S$. In all, we have two hyperparameters in iMixer, h_r and n . The pseudo-code of the iMLP module is provided in Appendix C.1.

5.1 CIFAR-10

To evaluate the performance of our iMixer model, in this subsection we conduct thorough experiments on the scratch training of the model with CIFAR-10. The statistics of the results are obtained by ten trials with random initialization through all the experiments, unless otherwise stated. We also perform the hyperparameter search with iMixer-S, and with those results in hand, we will consider additional studies in the following subsections.

Training. We use the CIFAR-10 dataset [33], which consists of 60,000 natural images of size 32×32 . The ground-truth object category labels are attached to each image and the number of categories is 10, with 6,000 images per class. There are 50,000 training images and 10,000 test images. For the training setting, we basically follow the previous study [3]. The images are resized to 224×224 and the AdamW [35] optimizer is used. We take the base learning rate $\frac{\text{batch size}}{512} \times 5 \times 10^{-4}$. The batch sizes for Small, Base and Large models are 512, 256 and 64, respectively. As the regularization method, we employ label smoothing [36] and stochastic depth [37]. As for the data augmentation, we apply cutout [38], cutmix [39], mixup [40], random erasing [41], and randaugment [42]. For more details, see Appendix C.2. We train iMixer and the vanilla Mixer in the exact same training configuration for fair comparison. All the experiments are conducted with four Quadro RTX 8000 GPU cards.

Results. Table 1 shows the results. Our iMixer models consistently improve the performance of the baseline vanilla Mixer models. The hyperparameters are taken as $h_r = 2$ and $n = 2$. The results for hyperparameter search is also provided in Table 2. All the results in these tables are obtained from the scratch training on the models. As for the prediction accuracy, one finds that the best hyperparameters are $h_r = 2$ and $n = 2$, while $n = 1$ already provides the competitive result. We will make comments regarding this observation with connection to the residual networks below and in the next subsection.

Table 2: Hyperparameter search for h_r and n in iMixer-S. Each slot represents the corresponding top-1 accuracy (%).

h_r	$n = 1$	$n = 2$	$n = 4$
0.25	88.26 \pm 0.28	88.22 \pm 0.33	88.29 \pm 0.37
0.5	88.32 \pm 0.39	88.21 \pm 0.45	88.22 \pm 0.43
1	88.36 \pm 0.31	88.32 \pm 0.32	88.32 \pm 0.32
2	88.54 \pm 0.34	88.56 \pm 0.30	88.46 \pm 0.26

From Table 1, we observe that the iMixer-L shows the largest improvement of the performance. In addition, Table 2 tells us that the larger the models become, the performance tends to be more improved from the vanilla Mixer models since the bigger h_r yields larger width in the hidden layers. These observations are in a sense counterintuitive since, as MLP-Mixer (including our iMixer) has much less inductive bias than state-of-the-art neural networks such as CNN, the models with more parameters seem to get more overfitted with small training data, such as CIFAR-10. Another aspect that can be observed in Table 1 is the milder degradation of performance from Small to Large in our

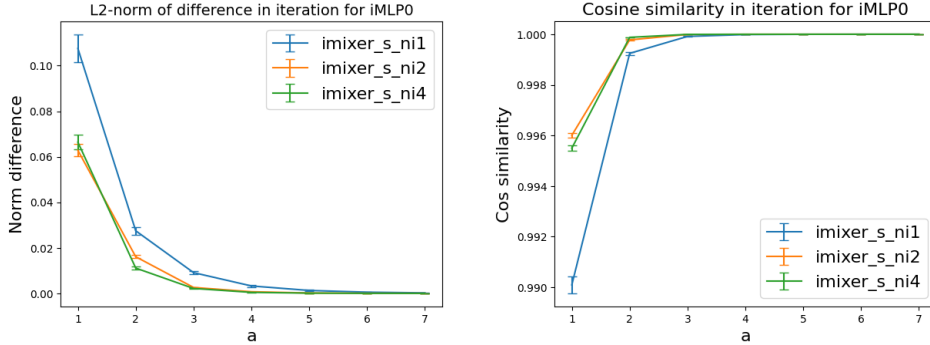


Figure 3: Convergence rate of L_2 -norm (left), $\|x^{a+1} - x^a\|$, and cosine similarity (right), $\cos(x^{a+1}, x^a)$, between two successive feature vectors in fixed-point iteration FPA in the iMLP module of the first layer (iMLP-0).

Table 3: Ablation study for the spectral normalization in iMixer-S ($h_r = 2$), trained on CIFAR-10. Each slot represents the corresponding top-1 accuracy (%).

Norm	$n = 1$	$n = 2$	$n = 4$
SpecNorm	88.54 \pm 0.34	88.56 \pm 0.30	88.46 \pm 0.26
w/o SpecNorm	88.73 \pm 0.39	88.32 \pm 0.31	88.07 \pm 0.28
BatchNorm	87.60 \pm 0.34	81.62 \pm 1.98	81.83 \pm 2.00

iMixer compared to the vanilla Mixer. These counterintuitive behaviors imply that our iMLP module, derived from a Hopfield-type neural network, is effective.

Table 2 does not show a significant statistical difference between $n = 1, 2$, and 4. This observation rather suggests that increasing the order n within these experiments does not significantly affect the performance of the models. In other words, while residual networks are indeed efficient neural network architectures, iMixer with larger $n = 2$ and 4 also exhibits competitive performance compared to $n = 1$. This implies the effectiveness of the i-Res module implementation in the proposed iMLP module and hence the validity of the formulation through the Hopfield/Mixer correspondence.

Nevertheless, $n = 1$ generically does not suffice for the accuracy of the expansion approximation FPA, Eq. (29), in the iMLP module. Figure 3 shows L_2 -norm and cosine similarity between two successive feature vectors x^{a+1} and x^a in iteration. The inputs are 16 test samples of CIFAR-10 chosen at random, and the L_2 -norm is normalized by the internal dimensions due to its scaling. The model names `imixer_s_ni*` indicate the trained iMixer-S models with $h_r = 2$ and the number of fixed-point iteration $n = 1, 2$ and 4, respectively. We observe that the models `imixer_s_ni2` and `imixer_s_ni4` yield approximately same convergence rate and $n = 2$ or 4 suffice for the expansion approximation, whereas $n = 1$ is not enough. We here show the result of the first layer in iMixer, iMLP-0. The plots corresponding to iMLP modules of other layers are given in Appendix C.3.

5.2 Ablation study

As already mentioned, the iMLP module actually involves the spectral normalization to make the backward operation $(1 - F)^{-1}$ a usual forward network as in Eq. (30). We study the effect of the spectral normalization by replacing the normalization condition, instead of changing the parameters n_p and c . While searching for optimal n_p and c could be beneficial, it appears to deviate from our paper’s primary objective. From Table 3, one can see that the replacement of the spectral normalization (SpecNorm) with the batch normalization (BatchNorm) apparently made worse the prediction accuracy of the model, where for the $n = 4$, Norm=BatchNorm case, we reduced the batch size because we encountered a memory issue when the original batch size is used in our environment. One may find from Table 3 that for $n = 1$ the model performance seems to slightly improve when the spectral normalization is removed (w/o SpecNorm). This is actually not the case for $n = 2$ and 4,

Table 4: First three lines show sample size and the number of classes for each dataset. The last two rows show the top-1 accuracy (%) of the vanilla Mixer-S and iMixer-S ($h_r = 2, n = 2$) trained on the corresponding dataset. Ten runs for each, except for ImageNet-1k.

	CIFAR-100	Stanford Cars	Food-101	ImageNet-1k
Train size	50,000	8,144	75,750	1,281,167
Test size	10,000	8,041	25,250	50,000
#Classes	100	196	101	1,000
Mixer-S	68.13 \pm 0.46	8.09 \pm 0.45	76.11 \pm 0.32	73.91
iMixer-S	68.26 \pm 0.30	7.96 \pm 0.17	76.08 \pm 0.20	74.10

rather larger n makes the performance worse. This tendency is consistent with the role of the spectral normalization in the i-Res module. This indicates that the spectral normalization is inevitable for the fixed-point iteration taken in the iMLP module, while the FPA turns out to be a naive residual connection for the $n = 1$ case. Thus, we can conclude that the spectral normalization is necessary for the assurance of the performance.

5.3 Other datasets

We also investigate the effectiveness of our iMixer for other datasets. We here utilize the commonly used datasets such as CIFAR-100 [33], Stanford Cars [43], Food-101 [44], and ImageNet-1k [45]. Table 4 shows the results of scratch training on the vanilla Mixer-S and iMixer-S models, and also provides the details on the datasets. The training configuration is taken exactly the same as in the previous subsections. From this table, one finds that our iMixer models show reasonably the competitive performance compared to the corresponding vanilla Mixer models. An exception is for the Stanford Cars dataset, which is composed of only 8,144 training samples and 8,041 test samples labeled with 196 classes. This result indicates that the scratch training both on the vanilla Mixer and on iMixer failed for such a too small sample size with relatively large number of classes. Table 4 shows that iMixer exhibits the competitive performance as a novel model of MetaFormer, which is consistent with the results shown in Table 1.

6 Discussion

6.1 Limitation

One limitation is the lack of application of iMixer for other computer vision tasks, such as segmentation, anomaly detection, and robustness, while including those discussions may make our main contributions obscure.

Another limitation is seen in the fixed number of hidden layers in our formulation of iMixer, in view of the hierarchical Hopfield network. In this paper we have only considered the case of three layers in total, while the formulation of iMixer can be generalized to any number of layers as given in Appendix B. To include more hidden layers would give us more supports and variations for the correspondence between the Hopfield networks and the iMixer.

A narrow focus on the Lagrangians in the formulation is another limitation. The Lagrangians for hidden neurons (in other words, activation functions f and e in Sec. 4.1) are actually not restricted along the derivation of iMixer, where we fixed $f = e = \text{GELU}$ just for practical reasons. Reconsideration of the Lagrangians for hidden neurons might give some more insights in understanding of the role of token mixers in MetaFormers. We leave these aspects of study for future works.

6.2 Conclusion

We proposed a generalized Hopfield/Mixer correspondence and found iMixer, invertible, implicit and iterative MLP-Mixer, as the counterpart of the hierarchical modern Hopfield network. The proposed iMLP module is an example of implicit layer that includes the deep equilibrium model. Although the primary interest of this paper is not intended to improve the accuracy of the state-of-the-art architecture, but to give a unified description for architecture design of MetaFormers such

as MLP-Mixer, we also provided the empirical evaluation. The evaluation experiments showed that iMixer performs reasonably well compared to the baselines and that the proposed model works.

iMixer involves MLP layers that propagate forward from the output side to the input side. Although this architectural design of iMixer may seem unconventional from a computer vision perspective, the empirical studies show that the larger the models become, the performance tends to be more improved from the vanilla Mixer models. Despite having less inductive bias than state-of-the-art neural networks like CNN, iMixer exhibits a somewhat counterintuitive trend where larger models with more parameters tend to perform better, even with limited training data that could potentially cause overfitting. This counterintuitive behavior suggests that exploring the correspondence between Hopfield networks and Mixer models could be a promising direction for describing MetaFormers more comprehensively.

References

- [1] Vaswani, A., N. Shazeer, N. Parmar, et al. Attention is all you need. In *Advances in Neural Information Processing Systems*, vol. 30. 2017.
- [2] Dosovitskiy, A., L. Beyer, A. Kolesnikov, et al. An Image is Worth 16x16 Words: Transformers for Image Recognition at Scale. In *International Conference on Learning Representation*. 2021.
- [3] Touvron, H., M. Cord, M. Douze, et al. Training data-efficient image transformers & distillation through attention. In *International Conference on Machine Learning*. 2021.
- [4] Tolstikhin, I. O., N. Houlsby, A. Kolesnikov, et al. Mlp-mixer: An all-mlp architecture for vision. *Advances in Neural Information Processing Systems*, 34, 2021.
- [5] Melas-Kyriazi, L. Do you even need attention? a stack of feed-forward layers does surprisingly well on imagenet. *arXiv preprint arXiv:2105.02723*, 2021.
- [6] Yu, W., M. Luo, P. Zhou, et al. Metaformer is actually what you need for vision. In *Proceedings of the IEEE/CVF conference on computer vision and pattern recognition*, pages 10819–10829. 2022.
- [7] Yu, W., C. Si, P. Zhou, et al. Metaformer baselines for vision. *IEEE Transactions on Pattern Analysis and Machine Intelligence*, 2023.
- [8] Hopfield, J. J. Neural networks and physical systems with emergent collective computational abilities. *Proceedings of the National Academy of Sciences*, 79(8):2554–2558, 1982.
- [9] —. Neurons with graded response have collective computational properties like those of two-state neurons. *Proceedings of the National Academy of Sciences*, 81(10):3088–3092, 1984.
- [10] Krotov, D., J. J. Hopfield. Large associative memory problem in neurobiology and machine learning. In *International Conference on Learning Representations*. 2021.
- [11] Ramsauer, H., B. Schäfl, J. Lehner, et al. Hopfield networks is all you need. In *International Conference on Learning Representations*. 2021.
- [12] Tang, F., M. Kopp. A remark on a paper of krotov and hopfield [arxiv: 2008.06996]. *arXiv preprint arXiv:2105.15034*, 2021.
- [13] Krotov, D. Hierarchical associative memory. *arXiv preprint arXiv:2107.06446*, 2021.
- [14] Behrmann, J., W. Grathwohl, R. T. Chen, et al. Invertible residual networks. In *International Conference on Machine Learning*, pages 573–582. PMLR, 2019.
- [15] Bai, S., J. Z. Kolter, V. Koltun. Deep equilibrium models. *Advances in Neural Information Processing Systems*, 32, 2019.
- [16] El Ghaoui, L., F. Gu, B. Travacca, et al. Implicit deep learning. *SIAM Journal on Mathematics of Data Science*, 3(3):930–958, 2021.

- [17] Touvron, H., P. Bojanowski, M. Caron, et al. Resmlp: Feedforward networks for image classification with data-efficient training. *IEEE Transactions on Pattern Analysis and Machine Intelligence*, 2022.
- [18] Liu, R., Y. Li, L. Tao, et al. Are we ready for a new paradigm shift? a survey on visual deep mlp. *Patterns*, 3(7):100520, 2022.
- [19] Rao, Y., W. Zhao, Z. Zhu, et al. Global filter networks for image classification. *Advances in neural information processing systems*, 34:980–993, 2021.
- [20] Tatsunami, Y., M. Taki. Sequencer: Deep lstm for image classification. In *Advances in Neural Information Processing Systems*. 2022.
- [21] Han, K., Y. Wang, J. Guo, et al. Vision gnn: An image is worth graph of nodes. In *Advances in Neural Information Processing Systems*. 2022.
- [22] Krotov, D., J. J. Hopfield. Dense associative memory for pattern recognition. In *Advances in Neural Information Processing Systems*, vol. 29. 2016.
- [23] Demircigil, M., J. Heusel, M. Löwe, et al. On a model of associative memory with huge storage capacity. *Journal of Statistical Physics*, 168(2):288–299, 2017.
- [24] Krotov, D., J. J. Hopfield. Dense associative memory is robust to adversarial inputs. *Neural computation*, 30(12):3151–3167, 2018.
- [25] Widrich, M., B. Schäfl, M. Pavlović, et al. Modern hopfield networks and attention for immune repertoire classification. In *Advances in Neural Information Processing Systems*, vol. 33, pages 18832–18845. 2020.
- [26] Yang, Y., Z. Huang, D. Wipf. Transformers from an optimization perspective. In *Advances in Neural Information Processing Systems*. 2022.
- [27] Hoover, B., Y. Liang, B. Pham, et al. Energy transformer. *arXiv preprint arXiv:2302.07253*, 2023.
- [28] Winston, E., J. Z. Kolter. Monotone operator equilibrium networks. *Advances in neural information processing systems*, 33:10718–10728, 2020.
- [29] Bai, S., V. Koltun, Z. Kolter. Stabilizing equilibrium models by jacobian regularization. In *International Conference on Machine Learning*, pages 554–565. PMLR, 2021.
- [30] Bai, S., V. Koltun, J. Z. Kolter. Multiscale deep equilibrium models. *Advances in Neural Information Processing Systems*, 33:5238–5250, 2020.
- [31] Kawaguchi, K. On the theory of implicit deep learning: Global convergence with implicit layers. In *International Conference on Learning Representations (ICLR)*. 2021.
- [32] Agarwala, A., S. S. Schoenholz. Deep equilibrium networks are sensitive to initialization statistics. In *Proceedings of the 39th International Conference on Machine Learning*, vol. 162, pages 136–160. 2022.
- [33] Krizhevsky, A. Learning multiple layers of features from tiny images, 2009.
- [34] Wightman, R. Pytorch image models. <https://github.com/rwightman/pytorch-image-models>, 2019.
- [35] Loshchilov, I., F. Hutter. Decoupled weight decay regularization. In *International Conference on Learning Representations*. 2019.
- [36] Szegedy, C., V. Vanhoucke, S. Ioffe, et al. Rethinking the inception architecture for computer vision. In *Proceedings of the IEEE Conference on Computer Vision and Pattern Recognition (CVPR)*. 2016.
- [37] Huang, G., Y. Sun, Z. Liu, et al. Deep networks with stochastic depth. In *Computer Vision—ECCV 2016: 14th European Conference, Amsterdam, The Netherlands, October 11–14, 2016, Proceedings, Part IV 14*, pages 646–661. Springer, 2016.

- [38] DeVries, T., G. W. Taylor. Improved regularization of convolutional neural networks with cutout. *arXiv preprint arXiv:1708.04552*, 2017.
- [39] Yun, S., D. Han, S. J. Oh, et al. Cutmix: Regularization strategy to train strong classifiers with localizable features. In *Proceedings of the IEEE/CVF International Conference on Computer Vision (ICCV)*. 2019.
- [40] Zhang, H., M. Cisse, Y. N. Dauphin, et al. mixup: Beyond empirical risk minimization. In *International Conference on Learning Representations*. 2018.
- [41] Zhong, Z., L. Zheng, G. Kang, et al. Random erasing data augmentation. In *Proceedings of the AAAI conference on artificial intelligence*, vol. 34, pages 13001–13008. 2020.
- [42] Cubuk, E. D., B. Zoph, J. Shlens, et al. Randaugment: Practical automated data augmentation with a reduced search space. In *Proceedings of the IEEE/CVF conference on computer vision and pattern recognition workshops*, pages 702–703. 2020.
- [43] Krause, J., M. Stark, J. Deng, et al. 3d object representations for fine-grained categorization. In *4th International IEEE Workshop on 3D Representation and Recognition (3dRR-13)*. 2013.
- [44] Bossard, L., M. Guillaumin, L. Van Gool. Food-101 – mining discriminative components with random forests. In *European Conference on Computer Vision*. 2014.
- [45] Krizhevsky, A., I. Sutskever, G. E. Hinton. Imagenet classification with deep convolutional neural networks. In *Advances in Neural Information Processing Systems*, vol. 25. 2012.
- [46] Hou, Q., Z. Jiang, L. Yuan, et al. Vision permutator: A permutable mlp-like architecture for visual recognition. *IEEE Transactions on Pattern Analysis and Machine Intelligence*, 2022.

A Broader Impact

Our work provides a variant of MetaFormers through the update rule of the hierarchical modern Hopfield network equipped with the corresponding Lagrangians. From this point of view, we can further study the fundamental properties of the token-mixing modules in state-of-the-art models by mapping them to the dynamics of Hopfield networks, which are more transparent neural network models. In addition, this perspective enables us to explore more efficient and generalizable MetaFormer models in a transparent way, not in ad hoc ways from tasks to tasks.

Since our experiments were designed to verify the formulation of our proposed iMixer, we believe that our results do not directly cause harm to society, while they can be of use to develop new Transformer-type architectures. It is expected that a more promising Hopfield model with a set of Lagrangians and the associated energy functions will be a good starting point to pursue brand-new neural network models.

B A General Formulation of iMixer

In this appendix, we describe one of the most general formulations of the iMixer. We begin with the setup of Krotov’s hierarchical Hopfield network [13] with L layers in total, which consists of N_A ($A = 1, \dots, L$) neurons in each layer. This system is a straightforward generalization of the model discussed in Sec. 4 and basically given by the following components: $x^A(t) \in \mathbb{R}^{N_A}$ neurons at each layer, interaction matrices between the adjacent layers, $\xi^{(A,A-1)} \in \mathbb{R}^{N_A \times N_{A-1}}$, and activation functions

$$g^A : \mathbb{R}^{N_A} \rightarrow \mathbb{R}^{N_A}, \quad A = 1, \dots, L, \quad (31)$$

determined through Lagrangians $L^A : \mathbb{R}^{N_A} \rightarrow \mathbb{R}$ such that $g^A(x^A) = \partial L^A(x^A)/\partial x^A$. For more details, see [13, Sec. 3]. With these notations, the dynamical equations describing the system of neurons are

$$\tau_A \frac{dx^A(t)}{dt} = \xi^{(A,A-1)} g^{A-1}(x^{A-1}(t)) + \xi^{(A,A+1)} g^{A+1}(x^{A+1}(t)) - x^A(t), \quad (32)$$

with boundary conditions $g^0 \equiv 0$ and $g^{L+1} \equiv 0$. One can easily find that by taking $L = 3$ and seeing that $x^1 = v$, $x^2 = x$ and $x^3 = h$, the system produces the one discussed in the main text. In this appendix, we always have in mind that x^1 neurons only are the visible ones and x^L are the lowest hidden ones.

We here again consider the adiabatic limit, $\tau_1 \gg \tau_2 \gg \dots \gg \tau_L$, which means that the dynamics of the hidden neurons in lower layers is always much faster than that of in the higher layers. Then, the dynamical equations turn out to be

$$\tau_1 \frac{dx^1(t)}{dt} = \xi^{(1,2)} g^2(x^2(t)) - x^1(t), \quad (33)$$

$$x^A(t) = \xi^{(A,A-1)} g^{A-1}(x^{A-1}(t)) + \xi^{(A,A+1)} g^{A+1}(x^{A+1}(t)), \quad (34)$$

$$x^L(t) = \xi^{(L,L-1)} g^{L-1}(x^{L-1}(t)), \quad (35)$$

where A in the middle equation runs from 2 to $L - 1$. Now we take the Lagrangian for the x^1 neurons as

$$L^1(x^1) = \sqrt{\sum_{i=1}^{N_1} (x_i^1 - \bar{x}^1)^2}, \quad \bar{x}^1 = \frac{1}{N_1} \sum_i x_i^1. \quad (36)$$

Other Lagrangians for the hidden neurons actually need not be specified to derive the general formulation of iMixer. By following the same discussion as in Sec. 3.2 in the main text, the dynamical equation for the x^1 neurons eventually becomes

$$x^1(t+1) = x^1(t) + H^2(x^2(t)), \quad H^2 := \xi^{(1,2)} g^2(\cdot). \quad (37)$$

To solve this equation, we need a solution for the x^2 neurons, which can be obtained by the i-Res module method as follows. Using the above reduced dynamical equations from $A = L$ to $A = 2$ one-by-one, one eventually obtains the solution as

$$x^2(t) = (1 - F^2)^{-1}(G^1(x^1(t))), \quad (38)$$

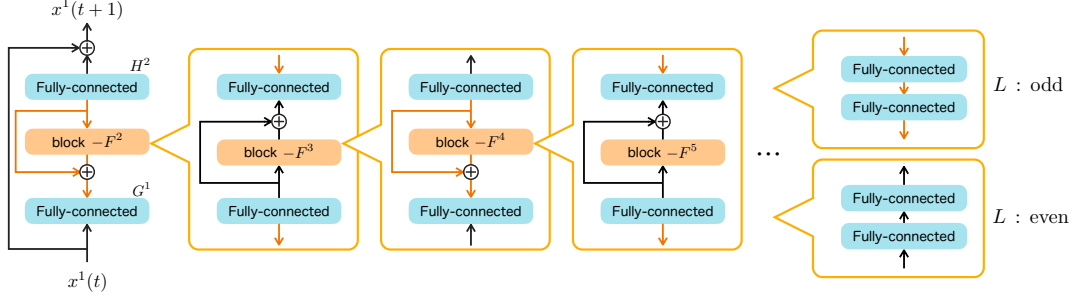


Figure 4: The structure of iMLP module for generic L .

where $F^A : \mathbb{R}^{N_A} \rightarrow \mathbb{R}^{N_A}$ are contractive MLP blocks defined as

$$F^A = H^{A+1} \circ (1 - F^{A+1})^{-1} \circ G^A, \quad A = 1, \dots, L-2, \quad (39)$$

$$F^{L-1} = H^L \circ G^{L-1}. \quad (40)$$

Fully-connected layers $G^A : \mathbb{R}^{N_A} \rightarrow \mathbb{R}^{N_{A+1}}$ and $H^{A+1} : \mathbb{R}^{N_{A+1}} \rightarrow \mathbb{R}^{N_A}$ are defined by

$$G^A = \xi^{(A+1,A)} g^A, \quad H^{A+1} = \xi^{(A,A+1)} g^{A+1}. \quad (41)$$

Thus, by substituting Eq. (38) to the discrete dynamical equation for the x^1 neurons, we obtain

$$x^1(t+1) = x^1(t) + F^1(x^1(t)), \quad (42)$$

with a hidden series of contractive MLP blocks F^A given as above; see Fig. 4. By utilizing the i-Res module method to the each $(1 - F^A)^{-1}$ and replacing the inverse operations with the fixed-point approximations FPA^A , we have a general iMixer architecture. Taking $L = 3$, one finds that this update rule for the x^1 neurons reproduces our iMLP module Eq. (30).

C Experimental Details

This section provides the experimental details, including the feature maps of the iMLP module.

C.1 Code of the iMLP module

The pseudo-code of the iMLP module is shown in Algorithm 2. As mentioned in the main text, we use PyTorch Image Models `timm` [34]³ for the implementation of the models. The iMixer models mostly have the same structure as the vanilla MLP-Mixer models, except for the use of this iMLP module for the token-mixing block. The module `spectral_norm_fc` in the code is the spectral normalization discussed and provided in [14].⁴

Algorithm 2 Pseudo-code of the invertible MLP layer, PyTorch-like code.

```
# MLP block with the invertible ResNet module
class iMlp(nn.Module):
    def __init__(self, d_vis, d_mid, d_hid, act=nn.GELU, drop=0.,
                 coeff=0.9, n_power=8, n_iter=2):
        super().__init__()
        self.fc1 = nn.Linear(d_vis, d_mid)
        self.fc_sn1 = spectral_norm_fc(nn.Linear(d_mid, d_hid),
                                       coeff, n_power)
        self.fc_sn2 = spectral_norm_fc(nn.Linear(d_hid, d_mid),
                                       coeff, n_power)
        self.fc2 = nn.Linear(d_mid, d_vis)

        self.act = act()
        self.drop = nn.Dropout(drop)
        self.n_iter = n_iter

    # feedforward operation with the i-Res module:
    # the fixed-point iteration method
    def forward(self, x):
        x = self.fc1(x)
        x_in = x
        for _ in range(self.n_iter):
            x = self.act(x)
            x = self.drop(x)
            x = self.fc_sn1(x)
            x = self.act(x)
            x = self.drop(x)
            x = self.fc_sn2(x)
            x = x + x_in
        x = self.act(x)
        x = self.drop(x)
        x = self.fc2(x)
        x = self.drop(x)
        return x
```

³<https://github.com/huggingface/pytorch-image-models>.

⁴<https://github.com/jhjacobson/invertible-resnet>.

C.2 Training details

We here report the detailed training setups commonly used for the vanilla MLP-Mixer and iMixer in Table 5. We basically follow the previous study [3], and also employ [46]⁵ for some considerations. The slashes indicate that the corresponding parameters are taken to the Small, Base, and Large models, respectively.

Table 5: Hyperparameters commonly used for the vanilla MLP-Mixer and our iMixer for fair comparison.

Training configuration	Small/Base/Large
optimizer	AdamW
training epochs	300
batch size	512/256/64
base learning rate	5e-4/2.5e-4/6.25e-5
weight decay	0.05
optimizer ϵ	1e-8
optimizer momentum	$\beta_1 = 0.9, \beta_2 = 0.999$
learning rate schedule	cosine decay
lower learning rate bound	1e-6
warmup epochs	20
warmup schedule	linear
warmup learning rate	1e-6
cooldown epochs	10
crop ratio	0.875
RandAugment	(9, 0.5)
mixup α	0.8
cutmix α	1.0
random erasing	0.25
label smoothing	0.1
stochastic depth	0.1/0.2/0.3

⁵<https://github.com/houqb/VisionPermutator>.

C.3 Convergence rate for fixed-point iteration in iMLP modules

We here show the convergence rate for fixed-point iterations in a trained iMixer-S, which has eight iMLP modules in total. The setup is exactly the same as in Fig. 3 in the main text; we consider L_2 -norm and cosine similarity between two successive feature vectors x^{a+1} and x^a of FPA in each iMLP module: $\text{Norm}_a := \|x^{a+1} - x^a\|/\sqrt{SC}$ and $\text{Cos}_a := \cos(x^{a+1}, x^a)$, where $S = 196$ and $C = 512$. A point is that the convergence rate of the fixed-point iteration method depends on samples and weights, which means in general the results differ samples by samples and layer by layer.

Below we provide the results for convergence rate of fixed-point iteration in each iMLP module. The inputs are 16 test samples of CIFAR-10. From these plots, we see that the first two layers show the clear difference between imixer_s_ni1 and imixer_s_ni2 or imixer_s_ni4, due to the detail of the input data. FPAs in middle layers converge relatively fast, probably since the middle layers mainly manipulate abstract features of the data, independent of the details. The final layer shows the large deviations, which implies the convergence rate differs for the classes sample by sample. In all, this results suggest it is challenging and unreasonable to completely determine the convergence rate of the iMLP modules.

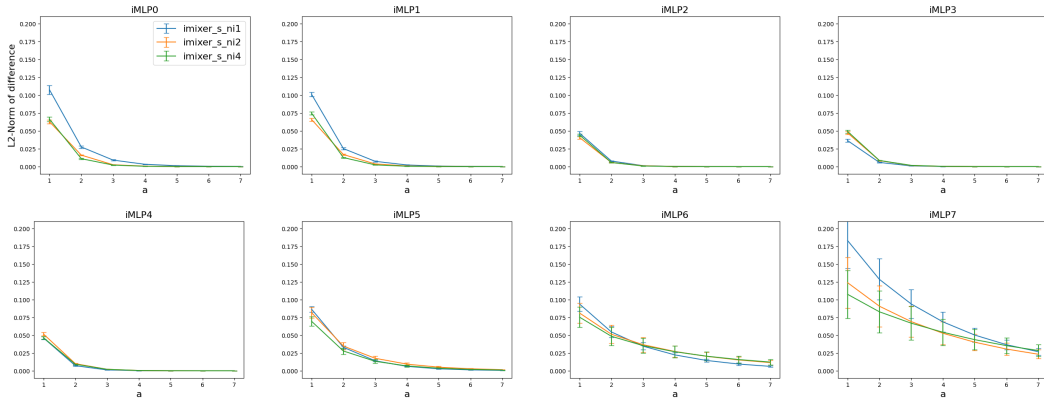


Figure 5: L_2 -norm differences in fixed-point iteration for iMLP modules. The vertical axis is Norm_a .

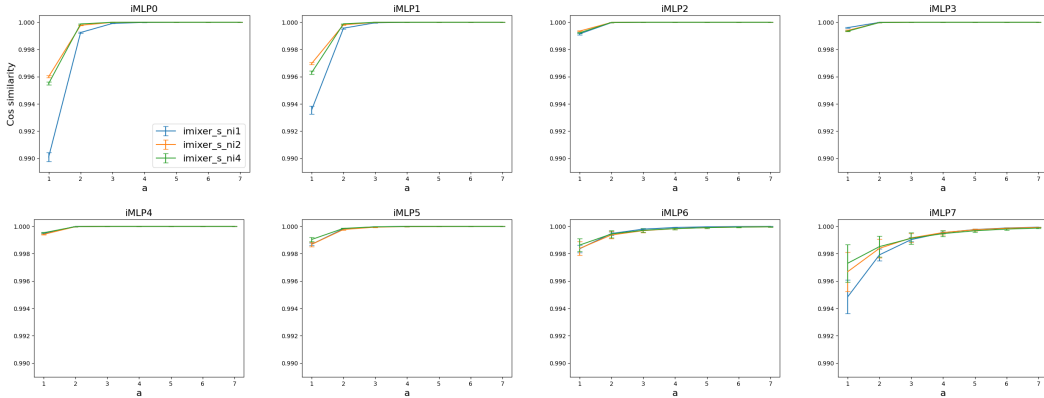
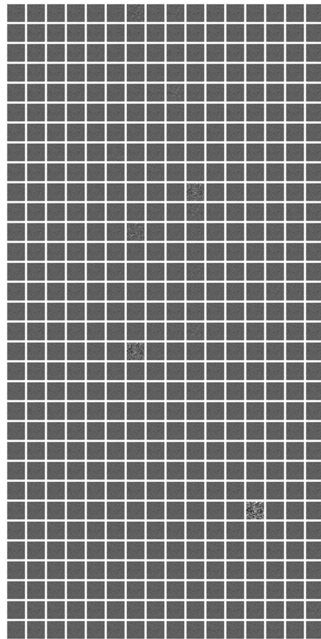


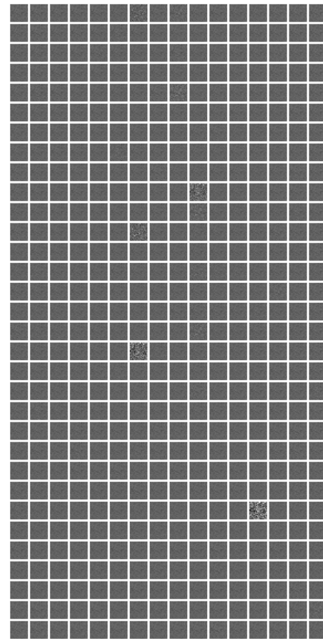
Figure 6: Cosine similarities in fixed-point iteration for iMLP modules. The vertical axis is Cos_a .

C.4 Feature maps

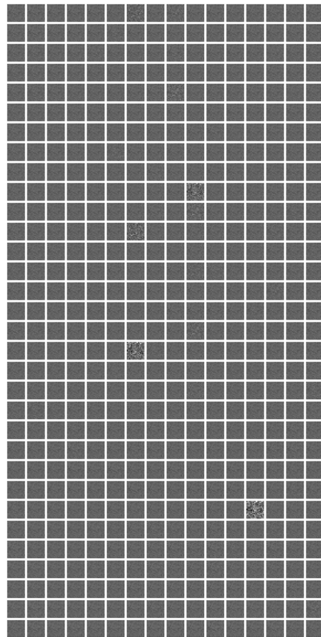
We provide a specific visualization of the feature maps of the fixed-point iteration below.



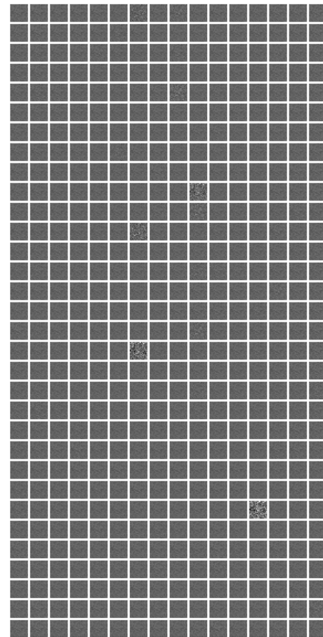
(a) At first iteration.



(b) At second iteration.



(c) At third iteration.



(d) At fourth (final) iteration.

Figure 7: Feature maps (outputs) of each fixed-point iteration at the final layer of iMixer-S with $h_r = 2$ and $n = 4$ trained on ImageNet-1k. An input image is a test sample of dog.